Two-electron capture from helium by fast α particles

Dževad Belkić,[1,2] Ivan Mančev,[3] and Mihajlo Mudrinić[2]
[1]*University of Stockholm, Atomic Physics, Frescativägen 24, S-104 05 Stockholm, Sweden*
[2]*Institute of Physics, P.O. Box 57, 11001 Belgrade, Yugoslavia*
[3]*Department of Physics, University of Niš, P.O. Box 91, 18001 Niš, Yugoslavia*
(Received 8 June 1993; revised manuscript received 6 December 1993)

Two-electron capture from helium by fast α particles is investigated. Working within the four-body framework of scattering theory, we perform detailed computations for differential as well as total cross sections, by means of the second-order Born distorted-wave approximation, and find good agreement with the available experimental data. We also report the results obtained by means of the continuum distorted-wave method in both the four-body formalism and the independent-particle model. The former fails to reproduce the measurement, whereas the latter emerges as a satisfactory method for α-He double-charge exchange. The reported study of the electronic continuum intermediate states clearly indicates that double-charge exchange is remarkably sensitive to inclusion of these long-range Coulomb effects, even at incident energies at which the Thomas double scattering is completely unimportant. This is in sharp contrast to the familiar situation at the comparable energies encountered in treating single-electron transfer in ion-atom collisions.

PACS number(s): 34.70.+e, 82.30.Fi

I. INTRODUCTION

Among atomic composite processes involving transitions of two or more electrons, multiple vacancy production was among the very first phenomena which were thoroughly investigated in the past. For a long period of time, theory for description of these problems was based exclusively upon the independent-particle model (IPM). For example, Hansteen and Mosebekk [1] used this general method to study multiple ionization in atomic collisions. Subsequently, McGuire and Weaver [2] further elaborated and extended the IPM to encompass combined processes, such as transfer ionization, transfer excitation, multiple excitation, and the like (see also Refs. [3–14]). Later, Gayet, Rivarola, and Salin [15] employed the IPM version of Cheshire's [16] continuum distorted-wave (CDW) approximation, accompanied by various models for the two-electron targets to study double-charge exchange. Their approach, with certain modifications, was utilized more recently in a number of examinations of two-electron capture [17–21]. The basic feature of all these previous investigations within the IPM and its variants is the preservation of the *three-body* formalism, despite the fact that the studied problems dealt with more than one active electron. Here, the total transition probability of a composite multielectron event is comprised of the binomial distribution of impact-parameter-dependent individual probabilities for each of the participating single-electron processes [1,2]. Static correlations, which are built in multielectron bound-state wave functions without any reference to collision, can be incorporated within certain modified versions of the IPM [11–15,17–21]. However, the IPM ignores altogether the genuine *many-body dynamics* of complex events from the onset and, therefore, discards a possibility for investigating electronic correlations as a participating *collisional* effect [22]. Hence it is clear that an appropriate many-body formalism should be a more natural starting point to treat the *static* and *dynamic* correlations on the same footing. Guided by this argument, several four-body versions of distorted-wave theories have recently been proposed to study two-electron transitions in scattering of completely stripped projectiles on heliumlike atomic systems [23,24] or in collisions between two hydrogenic atoms [25]. For example, the work of Gravielle and Miraglia [24] was aimed at developing the impulse approximation for double-charge exchange. Their method, however, violates the correct boundary conditions in the channel where the continuum intermediate states are taken into account. This is always the case in the standard formulation of the impulse approximation, as thoroughly discussed in the review paper by Belkić, Gayet, and Salin [26].

Recently, Belkić and Mančev [23,27] devised a strict extension of Cheshire's [16] CDW theory to double-charge exchange without any further approximations. The prior and post forms of the transition amplitudes in this CDW method are given by the matrix elements $T_{if}^{\mathrm{CDW}-}=\langle\chi_f^-|U_i|\chi_i^+\rangle$ and $T_{if}^{\mathrm{CDW}+}=\langle\chi_f^-|U_f^\dagger|\chi_i^+\rangle$, where $U_{i,f}\equiv U_{i,f}^{\mathrm{CDW}}=V_{i,f}-W_{i,f}^{\mathrm{CDW}}$. Here, the distorted waves $\chi_{i,f}^{\pm}\equiv\chi_{i,f}^{\mathrm{CDW}\pm}$ are expressed as the product of $\varphi_{i,f}$ with the three Coulomb waves (two for the electronic and one for the nuclear motion), where $\varphi_{i,f}$ are the initial and final bound states. The distorting potentials $W_{i,f}^{\mathrm{CDW}}$ are defined as the difference between the standard channel perturbations $V_{i,f}$ and the operators $\sum_{k=1}^{2}\nabla_k\varphi_{i,f}\cdot\nabla_k$. Such a four-body CDW method (CDW-4B) obeys the well-known asymptotic convergence criteria of Dollard [28] for Coulombic potentials. Computations of the total cross sections $Q_{if}^{\mathrm{CDW\text{-}4B}}$ performed in Refs. [23,27] for formation of H^- in H^+-He collision showed excellent agreement with experimental data. These results for $Q_{if}^{\mathrm{CDW\text{-}4B}}$

vary within 40% for several different choices of the two-electron bound-state wave functions $\varphi_{i,f}$, similarly to the case of single-charge exchange [29]. The distorted-wave functions $\chi_{i,f}^{\mathrm{CDW}\pm}$ are not normalized in both the three- and four-body formalisms at *finite* values of the interaggregate distances $r_{i,f}$.

This is in contrast to the boundary-corrected four-body first Born (CB1) approximation [30,31], which deals only with the normalized wave functions $\chi_{i,f}^{\pm}$. The scattering state vectors $\chi_{i,j}^{\mathrm{CB1}\pm}=\Phi_{i,f}^{\pm}$ of the CB1 model are simply given by the product of the unperturbed channel states $\Phi_{i,f}$ and the logarithmic distortion phase factors $\mathcal{F}_{i,f}^{\pm}$, due to the Coulomb long-range remainders of the perturbation potentials. For a given incident velocity, the eikonal phases $\mathcal{F}_{i,f}^{\pm}$ depend only upon the variables $\mathbf{r}_{i,f}$. The form of the functions $\mathcal{F}_{i,f}^{\pm}$ must be consistent with the distorting potentials $U_{i,f}^{\mathrm{CB1}}=V_{i,f}-V_{i,f}^{a}$, which are simple *multiplicative* operators. Here, $V_{i,f}^{a}$ are the usual asymptotic expressions of the channel perturbations $V_{i,f}$ at infinitely large values of $r_{i,f}$. Hence, in the transition amplitudes $T_{if}^{\mathrm{CB1}\pm}=\langle\Phi_f^{-}|V_{i,f}-V_{i,f}^{a}|\Phi_i^{+}\rangle$ of the CB1 approach, the pure *electronic* continuum intermediate states are ignored in both channels.

The four-body boundary-corrected continuum intermediate state (BCIS) approximation is a second-order model for two-electron capture which has recently been introduced by Belkić [32]. The perturbation potential $U_i^{\mathrm{BCIS}}=U_i^{\mathrm{CB1}}$, contained in the transition amplitude $T_{if}^{\mathrm{BCIS}}=\langle\chi_f^{\mathrm{CDW}-}|U_i^{\mathrm{CB1}}|\chi_i^{\mathrm{CB1}+}\rangle$, and the pertinent distorted wave $\chi_i^{\mathrm{BCIS}+}=\chi^{\mathrm{CB1}+}=\Phi_i^{+}$ are the same as in the CB1 model. The treatment of the exit channel, however, is identical to that of the CDW method, with the same distorted wave $\chi_f^{\mathrm{BCIS}-}=\chi_f^{\mathrm{CDW}-}$ and the associate distorting potential $W_f^{\mathrm{BCIS}}=W_f^{\mathrm{CDW}}$. This latter operator, however, does not appear explicitly in the expressions for $T_{if}^{\mathrm{BCIS}-}$ and $T_{if}^{\mathrm{CDW}-}$. An analogous and symmetric situation is encountered in the post form of the transition amplitude: $T_{if}^{\mathrm{BCIS}+}=\langle\chi_f^{\mathrm{CB1}-}|U_f^{\mathrm{CB1}\dagger}|\chi_i^{\mathrm{CDW}+}\rangle$.

In the present work, we shall concentrate on alternative second-order four-body method with the correct boundary conditions, termed the Born distorted-wave (BDW) method [33]. It is yet another hybrid-type model, which is intermediate to the above CDW and CB1 approaches. The connection is, however, established in a manner which is different from that already seen in the BCIS model. Namely, the perturbation potential $U_i^{\mathrm{BDW}}=U_i^{\mathrm{CDW}}=V_i-W_i^{\mathrm{CDW}}$, which explicitly appears in the transition amplitude $T_{if}^{\mathrm{BDW}-}$ and the associated distorted-wave function $\chi_i^{\mathrm{BDW}+}=\chi_i^{\mathrm{CDW}+}$ coincide with the corresponding quantities of the CDW model: $T_{if}^{\mathrm{BDW}-}=\langle\chi_f^{\mathrm{CB1}-}|U_i^{\mathrm{CDW}}|\chi_i^{\mathrm{CDW}+}\rangle$. In the exit channel, however, the same analysis as in the CB1 method is adopted. Similarly, the prior version of the T matrix reads as $T_{if}^{\mathrm{BDW}+}=\langle\chi_f^{\mathrm{CDW}-}|U_f^{\mathrm{CDW}\dagger}|\chi_i^{\mathrm{CB1}+}\rangle$. If we chose to consider the same distorted waves $\chi_{i,f}^{\pm}$ in both the BCIS and BDW methods, then the essential difference between the transition amplitudes

$$T_{if}^{\mathrm{BCIS}-}=\langle\chi_f^{\mathrm{CDW}-}|U_i^{\mathrm{CB1}}|\chi_i^{\mathrm{CB1}+}\rangle$$

and

$$T_{if}^{\mathrm{BDW}+}=\langle\chi_f^{\mathrm{CDW}-}|U_f^{\mathrm{CDW}\dagger}|\chi^{\mathrm{CB1}+}\rangle$$

is in the perturbation potentials U_i^{CB1} and U_f^{CDW}, which are *directly* present in the transition amplitude as the weight function, when projecting the initial onto the final scattering state of the total system. In the BDW model, one encounters the typical gradient operator potentials $\sum_{k=1}^{2}\nabla_k\varphi_{i,f}\cdot\nabla_k$, which are familiar from the CDW approximation. The role of these perturbations in the BCIS method is played by the conventional first-Born-type multiplicative operators $V_{i,f}-V_{i,f}^{a}$, which are the same as in the CB1 approach. The BDW approximation introduces a normalized scattering state for every value of r_i or r_f in the channel, in which the reduction of the BDW to the CB1 model takes place. However, the two electrons are treated in an asymmetrical manner in the entrance and exit channel. Hence, from a direct comparison between the BDW and CDW approximations, we will learn whether the departure from the normalization and symmetry in treating double electronic continuum intermediate states in the initial and/or final states could have significant consequences while performing testing against experiment. Another useful piece of information which should be available from the present study is related to an assessment of sensitivity of cross sections for two-electron transfer to various choices of the distorting potentials as well as to different selections of the bound-state wave functions within the above-mentioned second-order methods. In addition, we perform a detailed comparison between the two versions of the CDW approximations, namely, the four-body formalism and the independent-particle model.

Atomic units will be used throughout unless stated otherwise.

II. THEORY

Consider the following typical double-charge exchange in fast collisions of completely stripped projectiles with heliumlike targets:

$$Z_P+(Z_T;e_1,e_2)_i\rightarrow(Z_P;e_1,e_2)_f+Z_T\ , \tag{2.1}$$

where Z_K is the charge of the Kth nucleus and $j(=i,f)$ is the collective label for the set of the usual quantum numbers. We shall label by $\mathbf{s}_{1,2}$ and $\mathbf{x}_{1,2}$ the position vectors of the electrons $e_{1,2}$ relative to Z_P and Z_T, respectively. In terms of these vectors, the interelectron distance r_{12} is given by $r_{12}=|\mathbf{s}_1-\mathbf{s}_2|\equiv s_{12}=|\mathbf{x}_1-\mathbf{x}_2|\equiv x_{12}$. Let further $\mathbf{R}$ be the vector of the internuclear axis directed from Z_T to Z_P. In the entrance channel, it is convenient to introduce $\mathbf{r}_i$ as the relative vector of Z_P with respect to the center of mass of $(Z_T;e_1,e_2)_i$. Symmetrically, $\mathbf{r}_f$ will denote the relative vector of Z_T with respect to the center of mass of $(Z_P;e_1,e_2)_f$ in the exit channel of process (2.1).

Exact prior $\mathcal{T}_{if}^{-}$ and post $\mathcal{T}_{if}^{+}$ transition amplitudes for process (2.1) are available from, e.g., the well-known distorted-wave *atomic* scattering theory [26]:

$$\mathcal{T}_{if}^{-}=\langle\Psi_f^{-}|U_i|\chi_i^{+}\rangle,\quad \mathcal{T}_{if}^{+}=\langle\chi_f^{-}|U_f^{\dagger}|\Psi_i^{+}\rangle\ , \tag{2.2a}$$

where $U_{i,f}=V_{i,f}-W_{i,f}$ and $|\Psi^{\pm}_{i,f}\rangle=(1+G^{\pm}U_{i,f})|\chi^{\pm}_{i,f}\rangle$. Here, $V_{i,f}$ are the perturbation potentials in the entrance and exit channel: $V_i=Z_PZ_T/R-Z_P/s_1-Z_P/s_2$ and $V_f=Z_PZ_T/R-Z_T/x_1-Z_T/x_2$. Distorting potential operators $W_{i,f}=w_{i,f}+W^d_{if}$ are comprised of certain short-range interactions $w_{i,f}$ and the remainders $W^d_{i,f}$, which contain a Coulombic field if the scattering aggregates are charged. The objects $G^{\pm}$ represent the total Green's operators $G^{\pm}=1/(E-H\pm i\varepsilon)$, where ε is an infinitesimally small positive number. The quantities E and H, respectively, denote the total energy and the full Hamiltonian of the system under study. The distorted waves $\chi^{\pm}_{i,f}$ from Eq. (2.2a) are introduced through

$$|\chi^{\pm}_{i,f}\rangle=\Omega^{\pm}_{i,f}|\Phi^{\pm}_{i,f}\rangle\equiv(1+G^{\pm}_{i,f}w_{i,f})|\Phi^{\pm}_{i,f}\rangle\ , \tag{2.2b}$$

with $\Omega^{\pm}_{i,f}$ being the Møller wave operators and $G^{\pm}_{i,f}=1/(E-H_{i,f}-W_{i,f}\pm i\varepsilon)$. The channel Hamiltonians $H_{i,f}$ are defined by $H_{i,f}=H-V_{i,f}$. The *asymptotic* channel states $\Phi^{\pm}_{i,f}$ read as follows: $\Phi^{+}_i=\varphi_i\exp[i\mathbf{k}_i\cdot\mathbf{r}_i+i\nu_i\ln(k_ir_i-\mathbf{k}_i\cdot\mathbf{r}_i)]$ and

$$\Phi^{-}_f=\varphi_f\exp[-i\mathbf{k}_f\cdot\mathbf{r}_f-i\nu_f\ln(k_fr_f-\mathbf{k}_f\cdot\mathbf{r}_f)]\ ,$$

where $\nu_i=Z_P(Z_T-2)/v$, $\nu_f=Z_T(Z_P-2)/v$, with v being the incident velocity. The initial and final bound-state wave functions are labeled by $\varphi_{i,f}$, whereas $\mathbf{k}_{i,f}$ denote the initial and final wave vectors, respectively. We shall hereafter discard the total Green's operators $G^{\pm}$ in Eq. (2.2a) and deduce the following approximate expressions $T^{\pm}_{if}$ for the exact amplitudes $\mathcal{T}^{\pm}_{if}$:

$$T^{-}_{if}=\langle\chi^{-}_f|U_i|\chi^{+}_i\rangle,\quad T^{+}_{if}=\langle\chi^{-}_f|U^{\dagger}_f|\chi^{+}_i\rangle\ . \tag{2.2c}$$

We will presently be concerned only with the prior form of the transition amplitude. An extension of the analysis to the post version of the formalism can be accomplished in a symmetric and straightforward manner. Let us first search for the distorted wave χ^{+}_i in the factorized form: $\chi^{+}_i=\varphi_i\zeta^{+}_i$. The auxiliary function ζ^{+}_i is to be determined according to a particular choice of the distorting potential U_i. Substituting this ansatz for χ^{+}_i into Eq. (2.2b) and letting $\varepsilon\to0$, it will follow in the eikonal limit:

$$\begin{aligned}\zeta^{+}_i=&\mu_i^{-2i\nu_P}\mathcal{N}^{+}(\nu_{PT})[N^{+}(\nu_P)]^2e^{i\mathbf{k}_i\cdot\mathbf{r}_i}\\&\times{}_1F_1(-i\nu_{PT},1,ik_ir_f+i\mathbf{k}_i\cdot\mathbf{r}_f)\\&\times{}_1F_1(i\nu_P,1,ivs_1+i\mathbf{v}\cdot\mathbf{s}_1){}_1F_1(i\nu_P,1,ivs_2+i\mathbf{v}\cdot\mathbf{s}_2)\ ,\end{aligned} \tag{2.3a}$$

provided that U_i is chosen as

$$U_i\chi^{+}_i=-\zeta^{+}_i(E_i-H_T)\varphi_i-\sum_{k=1}^{2}\nabla_{x_k}\varphi_i\cdot\nabla_{s_k}\zeta^{+}_i\ , \tag{2.3b}$$

where μ_i is the reduced mass of the projectile and the target. Here, the symbol ${}_1F_1$ denotes the conventional confluent hypergeometric function and $N^{\pm}(\nu_K)=\Gamma(1\mp i\nu_K)e^{\pi\nu_K/2}$, $\mathcal{N}^{\pm}(\nu_{PT})=\Gamma(1\pm i\nu_{PT})e^{-\pi\nu_{PT}/2}$, with $\nu_{PT}=Z_PZ_T/v$ and $\nu_K=Z_K/v(K=P,T)$. We label by E_i the "exact" electronic binding energy of the target. The target Hamiltonian H_T is given by the sum of the two electronic kinetic energy operators and the potential $V_T=-Z_T/x_1-Z_T/x_2+1/x_{12}$. If φ_i were an *exact* bound-state wave function of the two-electron target, the first term $\zeta^{+}_i(H_T-E_i)\varphi_i\equiv\zeta^{+}_i\varphi'_i$ in (2.3b) would vanish identically. Since this is never the case in practice, the term φ'_i should generally be kept throughout, as originally suggested by Belkić [30] in the CB1 method. Given Eq. (2.3a), it is immediately verified that the distorted wave χ^{+}_i exhibits the proper eikonal asymptotic behavior: $\chi^{+}_i\xrightarrow[r_i\to\infty]{}\Phi^{+}_i$. The distorted wave χ^{-}_f in the exit channel will be looked for in a form which singles out the final bound state φ_f, namely, $\chi^{-}_f=\varphi_f\zeta^{-}_f$. Inserting this expression into (2.2b), allowing ε to approach zero, and using the eikonal hypothesis will imply

$$\zeta^{-}_f=\mathcal{N}^{-}(\nu_f)e^{-i\mathbf{k}_f\cdot\mathbf{r}_f}{}_1F_1(i\nu_f,1,-ik_fr_i-i\mathbf{k}_f\cdot\mathbf{r}_i)\ , \tag{2.4a}$$

subject to $W_f\chi^{-}_f=\zeta^{-}_f(E_f-H_P)\varphi_f+Z_T(Z_P-2)r_i^{-1}\chi^{-}_f$, or equivalently

$$U_f\chi^{-}_f=-\zeta^{-}_f(E_f-H_P)\varphi_f+Z_T\left[\frac{2}{r_i}-\frac{1}{x_1}-\frac{1}{x_2}\right]\chi^{-}_f\ , \tag{2.4b}$$

where, in general, the first term gives a nonzero contribution, due to unavailability of the exact bound-state wave function φ_f of the two-electron atomic system $(Z_P;e_1,e_2)_f$. The quantity E_f denotes the "exact" energy of the final bound state. The Hamiltonian H_P of the atomic system $(Z_P;e_1,e_2)_f$ is given by the sum of the two electronic kinetic energies and $V_P=-Z_P/s_1-Z_P/s_2+1/s_{12}$. The reduced mass of the two aggregates $(Z_P;e_1,e_2)_f$ and Z_T is denoted by μ_f. The distorted wave χ^{-}_f obeys the correct boundary condition, since it follows from Eq. (2.4a) that $\chi^{-}_f\xrightarrow[r_f\to\infty]{}\Phi^{-}_f$.

The choices (2.3b) and (2.4b) of the potentials $U_{i,f}$ determines the Born distorted-wave approximation [33]. Clearly, it is a hybrid-type model which in the entrance and exit channel coincides, respectively, with the CDW and CB1 method. The total cross section Q^{BDW}_{if} for reaction (2.1) is introduced by

$$Q^{\mathrm{BDW}}_{if}(a_0^2)=\int d\boldsymbol{\eta}\left|\frac{T^{\mathrm{BDW}}_{if}(\boldsymbol{\eta})}{2\pi v}\right|^2=\int d\boldsymbol{\eta}\left|\frac{R^{\mathrm{BDW}}_{if}(\boldsymbol{\eta})}{2\pi v}\right|^2\ , \tag{2.5}$$

where the eikonal limit is employed and $T^{\mathrm{BDW}}_{if}\equiv T^{(\mathrm{BDW})-}_{if}$,

$$\begin{aligned}R^{\mathrm{BDW}}_{if}(\boldsymbol{\eta})=&-N_P\int\int\int d\mathbf{x}_1d\mathbf{x}_2d\mathbf{R}\,e^{i\mathbf{q}_P\cdot(\mathbf{s}_1+\mathbf{s}_2)+i\mathbf{q}_T\cdot(\mathbf{x}_1+\mathbf{x}_2)}(vR+\mathbf{v}\cdot\mathbf{R})^{-i\xi_T}\varphi^{*}_f(\mathbf{s}_1,\mathbf{s}_2)\\&\times\{{}_1F_1(i\nu_P,1,ivs_1+i\mathbf{v}\cdot\mathbf{s}_1){}_1F_1(i\nu_P,1,ivs_2+i\mathbf{v}\cdot\mathbf{s}_2)(E_i-H_T)\varphi_i(\mathbf{x}_1,\mathbf{x}_2)\\&+{}_1F_1(i\nu_P,1,ivs_2+i\mathbf{v}\cdot\mathbf{s}_2)\nabla_{x_1}\varphi_i(\mathbf{x}_1,\mathbf{x}_2)\cdot\nabla_{s_1}{}_1F_1(i\nu_P,1,ivs_1+i\mathbf{v}\cdot\mathbf{s}_1)\\&+{}_1F_1(i\nu_P,1,ivs_1+i\mathbf{v}\cdot\mathbf{s}_1)\nabla_{x_2}\varphi_i(\mathbf{x}_1,\mathbf{x}_2)\cdot\nabla_{s_2}{}_1F_1(i\nu_P,1,ivs_2+i\mathbf{v}\cdot\mathbf{s}_2)\}\ ,\end{aligned} \tag{2.6}$$

with $N_K=[N^+(\nu_K)]^2$, $\xi_K=2\nu_K=2Z_K/v$ $(K=P,T)$. Here we used the following eikonal relation: $\mathbf{k}_i\cdot\mathbf{r}_i+\mathbf{k}_f\cdot\mathbf{r}_f=\mathbf{q}_P\cdot(\mathbf{s}_1+\mathbf{s}_2)+\mathbf{q}_T\cdot(\mathbf{x}_1+\mathbf{x}_2)$, where $2\mathbf{q}_{P,T}=\pm\boldsymbol{\eta}-q^{\pm}\hat{\mathbf{v}}$ and $q^{\pm}=v\pm(E_f-E_i)/v$, with $\boldsymbol{\eta}=(\eta\cos\phi_\eta,\eta\sin\phi_\eta,0)$ being the transversal two-dimensional component of the momentum transfer. Matrix elements R_{if}^{BDW} are reduced to an easily obtainable triple numerical integration, by the same technique developed by Belkić [32] in the case of the BCIS approximation. In Eq. (2.5) the product $\mathcal{F}(\mathbf{R})$ $\equiv{}_1F_1(-i\nu_{PT},1,ik_ir_f+i\mathbf{k}_i\cdot\mathbf{r}_f){}_1F_1(-i\nu_f,1,ik_fr_i+i\mathbf{k}_f\cdot\mathbf{r}_i)$ is first reduced to its consistent eikonal form $\rho^{2i\nu_{PT}}(vR+\mathbf{v}\cdot\mathbf{r})^{-i\xi_T}$, where unimportant phase factors of the unit moduli are ignored. Here, $\boldsymbol{\rho}$ is the projection of vector $\mathbf{R}$ onto the XOY plane perpendicular to the incidence direction (Z axis), i.e., $\boldsymbol{\rho}=\mathbf{R}-\mathbf{Z}$, where $\boldsymbol{\rho}\cdot\mathbf{Z}=0$. The vector $\mathbf{Z}$ represents the projection of $\mathbf{R}$ onto the Z axis. A subsequent easy calculation shows that the phase factor $\rho^{2i\nu_{PT}}$, which directly stems from the internuclear potential $V_{PT}=Z_PZ_T/R$, finally disappears from Eq. (2.5). Hence this potential yields a vanishing contribution to the total cross section Q_{if}^{BDW} in the eikonal limit, as it should [26]. It ought to be recalled that the factor $\rho^{2i\nu_{PT}}$ does not disappear from the differential cross sections. This phase describes the Rutherford scattering [34,35], which plays a particularly important role at larger scattering angles (corresponding classically to close encounters). The differential cross sections are defined by the relation [26]

$$\frac{dQ_{if}^{\mathrm{BDW}}}{d\Omega}=\frac{\mu_i\mu_f}{4\pi^2}\frac{k_f}{k_i}|T_{if}^{\mathrm{BDW}}(\boldsymbol{\eta})|^2\left[\frac{a_0^2}{sr}\right], \tag{2.7}$$

where the ratio k_f/k_i is close to unity, since the heavy projectiles scatter mainly in the forward direction at high impact energies. The scattering angle θ is identified from the relation $\eta=2\mu_{PT}v\sin(\theta/2)$, where μ_{PT} is the reduced mass of the projectile and target nucleus. Calculation of the angular distributions $dQ_{if}^{\mathrm{BDW}}/d\Omega$ becomes particularly convenient in the BDW approximation, when either of the two-electron atoms is neutral, i.e., for $Z_P=2$ or $Z_T=2$. This is because the function $\mathcal{F}(\mathbf{R})$ reduces to the single term $(vR-\mathbf{v}\cdot\mathbf{R})^{i\xi_T}$ in $T_{if}^{-}(\boldsymbol{\eta})$ for $Z_P=2$ or to $(vR+\mathbf{v}\cdot\mathbf{R})^{i\xi_P}$ in $T_{if}^{+}(\boldsymbol{\eta})$ for $Z_T=2$, without any overall multiplying ρ term. Hence a trivial modification of the sign of the parameters $\xi_{P,T}$ as well as of the signs $\mp$ of the term $\mathbf{v}\cdot\mathbf{R}$ in the function $(vR\mp\mathbf{v}\cdot\mathbf{R})^{\xi_{P,T}}$ enables us to obtain both differential and total cross sections from the same algorithm associated with the BDW method.

In the next section, we shall make a comparison of the BDW method with the CB1, BCIS, and CDW approximations. Therefore we list below the prior forms of the transition amplitudes in these three latter models, which all employ the distorted waves $\chi_{i,f}^{\pm}$ in the forms $\varphi_{i,f}\zeta_{i,f}^{\pm}$. In the CB1 method [30,31], the choice of U_f and ζ_f^- is given by Eqs. (2.4a) and (2.4b), respectively. Here, the exit channel is specified in the following symmetric manner:

$$\zeta_i^+=\mathcal{N}^+(\nu_i)e^{i\mathbf{k}_i\cdot\mathbf{r}_i}{}_1F_1(-i\nu_i,1,ik_ir_f+i\mathbf{k}_i\cdot\mathbf{r}_f)\,, \tag{2.8a}$$

$$U_i\chi_i^+=-\zeta_i^+(E_i-H_T)\varphi_i+Z_P\left[\frac{2}{r_f}-\frac{1}{s_1}-\frac{1}{s_2}\right]\chi_i^+\,. \tag{2.8b}$$

This yields

$$R_{if}^{\mathrm{CB1}}(\boldsymbol{\eta})=\int\int\int d\mathbf{R}d\mathbf{s}_1d\mathbf{s}_2e^{i\mathbf{q}_P\cdot(\mathbf{s}_1+\mathbf{s}_2)+i\mathbf{q}_T\cdot(\mathbf{x}_1+\mathbf{x}_2)}(vR+\mathbf{v}\cdot\mathbf{R})^{-i\xi}\varphi_f^*(\mathbf{s}_1,\mathbf{s}_2)$$
$$\times\left[(H_T-E_i)\varphi_i(\mathbf{x}_1,\mathbf{x}_2)+Z_P\left[\frac{2}{r_f}-\frac{1}{s_1}-\frac{1}{s_2}\right]\varphi_i(\mathbf{x}_1,\mathbf{x}_2)\right], \tag{2.8c}$$

where $\xi=2(Z_T-Z_P)/v$. The expression (2.8c) is further reduced to a double or triple real numerical integration [30,31]. In the BCIS model [32], the pair $\{U_i,\chi_i^+\}$ is given by Eqs. (2.3a) and (2.3b), whereas the set $\{U_f,\chi_f^-\}$ is selected as

$$\zeta_f^-=\mu_f^{2i\nu_T}\mathcal{N}^-(\nu_{PT})[N^-(\nu_P)]^2e^{-i\mathbf{k}_f\cdot\mathbf{r}_f}{}_1F_1(i\nu_{PT},1,-ik_fr_i-i\mathbf{k}_f\cdot\mathbf{r}_i)$$
$$\times{}_1F_1(-i\nu_T,1,-ivx_1-i\mathbf{v}\cdot\mathbf{x}_1){}_1F_1(-i\nu_T,1,-ivx_2-i\mathbf{v}\cdot\mathbf{x}_2)\,, \tag{2.9a}$$

$$U_f\chi_f^-=-\zeta_f^-(E_f-H_P)\varphi_f-\sum_{k=1}^{2}\nabla_{s_k}\varphi_f\cdot\nabla_{x_k}\zeta_f^-\,. \tag{2.9b}$$

The corresponding matrix element in the BCIS approximation is then expressed by [32]

$$R_{if}^{\mathrm{BCIS}}(\boldsymbol{\eta})=N_T\int\int\int d\mathbf{R}d\mathbf{s}_1d\mathbf{s}_2e^{i\mathbf{q}_P\cdot(\mathbf{s}_1+\mathbf{s}_2)+i\mathbf{q}_T\cdot(\mathbf{x}_1+\mathbf{x}_2)}(vR-\mathbf{v}\cdot\mathbf{R})^{-i\xi_P}$$
$$\times\varphi_f^*(\mathbf{s}_1,\mathbf{s}_2){}_1F_1(i\nu_T,1,ivx_1+i\mathbf{v}\cdot\mathbf{x}_1){}_1F_1(i\nu_T,1,ivx_2+i\mathbf{v}\cdot\mathbf{x}_2)$$
$$\times\left[(H_T-E_i)\varphi_i(\mathbf{x}_1,\mathbf{x}_2)+Z_P\left[\frac{2}{r_f}-\frac{1}{s_1}-\frac{1}{s_2}\right]\varphi_i(\mathbf{x}_1,\mathbf{x}_2)\right]. \tag{2.9c}$$

Finally, the CDW method consists of symmetrical choices $\{U_i,\chi_i^+\}$ and $\{U_f,\chi_f^-\}$ as in Eqs. (2.3a) and (2.3b) and (2.9a) and (2.9b), respectively [23,27]. Therefore

$$R_{if}^{\mathrm{CDW}}(\eta)=-N_P N_T \int\int\int d\mathbf{x}_1 d\mathbf{x}_2 d\mathbf{R} e^{i\mathbf{q}_P\cdot(\mathbf{s}_1+\mathbf{s}_2)+i\mathbf{q}_T\cdot(\mathbf{x}_1+\mathbf{x}_2)} \varphi_f^*(\mathbf{s}_1,\mathbf{s}_2)\,{}_1F_1(i\nu_T,1,ivx_1+i\mathbf{v}\cdot\mathbf{x}_1)\,{}_1F_1(i\nu_T,1,ivx_2+i\mathbf{v}\cdot\mathbf{x}_2)$$
$$\times\{{}_1F_1(i\nu_P,1,ivs_1+i\mathbf{v}\cdot\mathbf{s}_1)\,{}_1F_1(i\nu_P,1,ivs_2+i\mathbf{v}\cdot\mathbf{s}_2)(E_i-H_T)\varphi_i(\mathbf{x}_1,\mathbf{x}_2)$$
$$+{}_1F_1(i\nu_P,1,ivs_2+i\mathbf{v}\cdot\mathbf{s}_2)\nabla_{x_1}\varphi_i(\mathbf{x}_1,\mathbf{x}_2)\cdot\nabla_{s_1}\,{}_1F_1(i\nu_P,1,ivs_1+i\mathbf{v}\cdot\mathbf{s}_1)$$
$$+{}_1F_1(i\nu_P,1,ivs_1+i\mathbf{v}\cdot\mathbf{s}_1)\nabla_{x_2}\varphi_i(\mathbf{x}_1,\mathbf{x}_2)\cdot\nabla_{s_2}\,{}_1F_1(i\nu_P,1,ivs_2+i\mathbf{v}\cdot\mathbf{s}_2)\}\ . \tag{2.10}$$

Both matrix elements R_{if}^{BCIS} and R_{if}^{CDW} can be expressed through three-dimensional numerical quadratures [23,27,32]. We point out that the computation of the differential cross section in the four-body CDW method becomes a laborious task, since it proceeds through the well-known formula [26]

$$\frac{dQ_{if}^{\mathrm{CDW}}}{d\Omega}=\left|iv\mu_{PT}\int_0^\infty d\rho\,\rho^{1+2i\nu_{PT}}\mathcal{A}_{if}^{\mathrm{CDW}}(\rho)J_{m_i-m_f}(\eta\rho)\right|^2\left[\frac{a_0^2}{sr}\right], \tag{2.11}$$

where $\mathcal{A}_{if}^{\mathrm{CDW}}(\rho)=\int_0^\infty d\kappa\,\kappa J_{m_i-m_f}(\kappa\rho)R_{if}^{\mathrm{CDW}}(\kappa)$. Here, $J_\nu(z)$ is the Bessel function of the first order and ν kind, whereas m_i and m_f are the magnetic quantum numbers of the initial and final bound states, respectively. Due to an additional double integration over ρ and κ, the cross sections (2.11) in the CDW approximation are obtained through the *five*-dimensional complicated quadratures over integrands, weighted with the two highly oscillating Bessel functions. The same drawback is also encountered in the CDW-EIS approximation, which treats the exit channel in the same manner as done in the CDW model, whereas the distorted wave of the entrance channel is given by the eikonal phase $\exp[i\nu_P\ln(vs_1+\mathbf{v}\cdot\mathbf{s}_1)+i\nu_P\ln(vs_2+\mathbf{v}\cdot\mathbf{s}_2)]$, accompanied by the appropriate distorting potential which appears directly in the prior transition amplitude $T_{if}^{\mathrm{CDW\text{-}EIS}}$. Here, EIS is an acronym for eikonal intermediate state. Due to this difficulty alone, encountered in the CDW and CDW-EIS models, it is advisable to search for other alternative distorted-wave methods along the lines of the BDW, BCIS, and similar approximations.

III. THE RESULTS OF THE NUMERICAL COMPUTATIONS

Here, we apply the BDW, CDW, and CB1 approximations to compute both the differential and total cross sections at high energies for the two-electron capture by α particles from helium:

$$^4\mathrm{He}^{2+}+{}^4\mathrm{He}(1s^2)\rightarrow{}^4\mathrm{He}(1s^2)+{}^4\mathrm{He}^{2+}\ . \tag{3.1}$$

There is no *post-prior* discrepancy for this reaction. The details about the numerical computations within the BDW method are similar to those explained in Ref. [32] for the BCIS approximation. The algorithms for the CDW and CB1 models are thoroughly discussed in Refs. [23,27,30,31]. Most of the present computations are performed by using the uncorrelated one-parameter orbitals of the Hylleraas type [36] in both the entrance and exit channel. For example, the initial bound state of the target is described by $\varphi_i(\mathbf{x}_1,\mathbf{x}_2)=(\gamma^3/\pi)e^{-\gamma(x_1+x_2)}$, where γ is the effective charge $\gamma=Z_T-\lambda$, with the parameter λ being the inner Slater screening ($\lambda=5/16=0.3125$). In such a case we have

$$\varphi_i'(\mathbf{x}_1,\mathbf{x}_2)\equiv(H_T-E_i)\varphi_i(\mathbf{x}_1,\mathbf{x}_2)$$
$$=\left[\frac{1}{x_{12}}-\frac{\lambda}{x_1}-\frac{\lambda}{x_2}+\Delta_i\right]\varphi_i(\mathbf{x}_1,\mathbf{x}_2)\ , \tag{3.2}$$

with $\Delta_i=E_i-\epsilon_i$ where $\epsilon_i=\gamma^2=-2.847\,656\,25$. The most precise variational calculations of Pekeris [37] is presently taken as the "exact" value E_i, which for helium becomes $\epsilon_i=-2.903\,724\,4$, so that $\Delta_i=-0.056\,068\,15$. If, for a given atomic system, a variational estimate is not available, one can use an experimental value for the "exact" energies E_i and E_f. The physical meaning of the correction φ_i' is obvious from the right-hand side of Eq. (3.2), where the correlation term $1/r_{12}$, missing from $\varphi_i(\mathbf{x}_1,\mathbf{x}_2)$, is reintroduced into the formalism, even though the uncoupled one-parameter Hylleraas [36] orbitals are employed from the onset. We emphasize that introducing the correction φ_i' makes the formulation of the boundary conditions intrinsically consistent, despite the use of the approximate bound-state wave functions $\varphi_{i,f}$ for two-electron systems. However, explicit computations are necessary in order to see whether this correction is numerically relevant or not. In Table I, we report the differential cross sections $dQ_{if}^{\mathrm{CB1(a)}}/d\Omega$ and $dQ_{if}^{\mathrm{CB1(b)}}/d\Omega$ of the CB1 approximation without and with the corrective term φ_i', respectively, at the incident energy 1.5 MeV. The two sets of results agree within 15% in a very close vicinity of the forward peak. The angular distribution $dQ_{if}^{\mathrm{CB1(a)}}/d\Omega$ exhibits a characteristic dip at the scattering angle $\theta_{\mathrm{lab}}\approx 0.1120$ mrad. The same type of dip is also recorded in $dQ_{if}^{\mathrm{CB1(b)}}/d\Omega$ at a slightly shifted angle $\theta_{\mathrm{lab}}\approx 0.1145$. In the dip region, the two cross sections differ by a factor which is of the order of 200, in the mesh shown in Table I. Away from this dip area, however, the two sets of results are in remarkably good agreement with each other and they become completely indistinguishable at angles above 0.5 mrad. The extremely sharp dip in $dQ_{if}^{\mathrm{CB1(a)}}$ is due to a strong cancellation of the opposite contributions coming from the repulsive $(2Z_P/R)$ and attractive $(-Z_P/s_1-Z_P/s_2)$ potentials in the matrix element (2.8c). This dip, however, remains virtually unmasked by inclusion of the eigenvalue-problem correction φ_i' into the cross section $dQ^{\mathrm{CB1(b)}}/d\Omega$. Most probably, the dip will be filled in by including the contribution from the excited states, as pre-

TABLE I. Differential cross sections $dQ_{if}^{\mathrm{CB1}}/d\Omega \equiv (dQ_{if}^{\mathrm{CB1}\pm}/d\Omega)_{\mathrm{lab}}$ (cm^2/sr) as a function of the scattering angle $\theta \equiv \theta_{\mathrm{lab}}$ (mrad) at incident energy $E_{\mathrm{lab}} = 1.5$ MeV for double-charge exchange (3.1). The columns (a) and (b) represent, respectively, the cross sections of the boundary-corrected first Born (CB1) approximation [30] without and with the correction (3.2). The last column is the ratio of the number in column (b) to the one in (a). Both sets (a) and (b) of the results are obtained by using the one-parameter Hylleraas [36] wave function $\varphi_{i,f}$ for helium. Notation: $x.y[-z] \equiv x.y \times 10^{-z}$.

	$\left[\frac{dQ_{if}^{CB1}}{d\Omega}\right]_{\mathrm{lab}}$ (cm^2/sr)				$\left[\frac{dQ_{if}^{CB1}}{d\Omega}\right]_{\mathrm{lab}}$ (cm^2/sr)		
θ_{lab} (mrad)	(a)	(b)	Ratio	θ_{lab} (mrad)	(a)	(b)	Ratio
0.0000	9.65[−12]	1.11[−11]	1.15	0.1550	6.23[−14]	5.54[−14]	0.89
0.0125	8.94[−12]	1.03[−11]	1.15	0.1600	6.55[−14]	5.91[−14]	0.90
0.0250	7.12[−12]	8.20[−12]	1.15	0.1650	6.75[−14]	6.17[−14]	0.91
0.0375	4.89[−12]	5.65[−12]	1.16	0.1700	6.85[−14]	6.31[−14]	0.92
0.0500	2.88[−12]	3.36[−12]	1.17	0.1750	6.86[−14]	6.37[−14]	0.93
0.0750	5.96[−13]	7.29[−13]	1.22	0.2000	6.05[−14]	5.77[−14]	0.95
0.1000	2.95[−14]	4.77[−14]	1.62	0.2250	4.76[−14]	4.60[−14]	0.97
0.1025	1.69[−14]	3.04[−14]	1.80	0.2500	3.58[−14]	3.49[−14]	0.97
0.1050	8.35[−15]	1.77[−14]	2.12	0.2750	2.66[−14]	2.61[−14]	0.98
0.1075	3.08[−15]	9.02[−15]	2.93	0.3000	1.98[−14]	1.95[−14]	0.98
0.1100	5.00[−16]	3.56[−15]	7.12	0.3250	1.49[−14]	1.47[−14]	0.99
0.1105	2.57[−16]	2.80[−15]	10.9	0.3500	1.13[−14]	1.12[−14]	0.99
0.1110	9.66[−17]	2.15[−15]	22.3	0.3750	8.69[−15]	8.63[−15]	0.99
0.1115	1.38[−17]	1.58[−15]	114.5	0.4000	6.78[−15]	6.74[−15]	0.99
0.1120	5.30[−18]	1.11[−15]	209.4	0.4250	5.36[−15]	5.33[−15]	0.99
0.1125	6.76[−17]	7.33[−16]	10.8	0.4500	4.28[−15]	4.27[−15]	0.997
0.1130	1.97[−16]	4.35[−16]	2.21	0.4750	3.46[−15]	3.44[−15]	0.997
0.1135	3.90[−16]	2.18[−16]	0.55	0.5000	2.82[−15]	2.82[−15]	1.0
0.1140	6.44[−16]	7.66[−17]	0.12	0.5500	1.93[−15]	1.93[−15]	1.0
0.1145	9.56[−16]	8.08[−18]	0.008	0.6000	1.37[−15]	1.37[−15]	1.0
0.1150	1.32[−15]	8.80[−18]	0.007	0.6500	9.94[−16]	9.94[−16]	1.0
0.1200	7.36[−15]	3.12[−15]	0.42	0.7000	7.37[−16]	7.37[−16]	1.0
0.1250	1.61[−14]	1.00[−14]	0.62	0.7500	5.65[−16]	5.65[−16]	1.0
0.1300	2.59[−14]	1.87[−14]	0.72	0.8000	4.27[−16]	4.27[−16]	1.0
0.1350	3.54[−14]	2.78[−14]	0.79	0.8500	3.42[−16]	3.42[−16]	1.0
0.1400	4.42[−14]	3.64[−14]	0.82	0.9000	2.84[−16]	2.84[−16]	1.0
0.1450	5.16[−14]	4.40[−14]	0.85	0.9500	1.91[−16]	1.91[−16]	1.0
0.1500	5.76[−14]	5.03[−14]	0.87	1.000	1.79[−16]	1.79[−16]	1.0

viously observed in the single-charge exchange problem treated within the CB1 model [38]. The total cross sections $Q_{if}^{\mathrm{CB1(a)}}$ and $Q_{if}^{\mathrm{CB1(b)}}$ computed using the CB1 model, without and with the φ_i' correction, respectively, at incident energies 100–6000 keV are shown in Table II. It is observed that the values of $Q_{if}^{\mathrm{CB1(b)}}$ are decreased in comparison to the values of $Q_{if}^{\mathrm{CB1(a)}}$ by a factor $\gamma \equiv Q_{if}^{\mathrm{CB1(b)}}/Q_{if}^{\mathrm{CB1(a)}} = 0.99-0.92$, at lower-intermediate energies ranging from 600 to 100 keV. The pattern is, however, reversed at higher energies belonging to the interval (600–6000] keV, at which $\gamma = 1.01-1.28$ (see Table II). This indicates that the electronic correlations become progressively more important as the incident energy increases. An analogous situation is also encountered in the case of single-electron capture from helium by bare nuclei, when comparing the cross sections due to some highly correlated wave functions [39,40] with the uncorrelated one-parameter Hylleraas [36] orbitals. The absolute magnitude of the difference of the two sets of the double-charge exchange data from the Table II, however, does not exceed 30%. Assuming that a similar conclusion would also hold true for the second-order theories

TABLE II. The same as in Table I, except for the total cross sections Q_{if}^{CB1} (cm^2) $\equiv Q_{if}^{\mathrm{CB1}\pm}$ (cm^2), as a function of the incident energy E_{lab} (keV).

	Q_{if}^{CB1} (cm^2)		
E_{lab} (keV)	(a)	(b)	Ratio
100	3.59[−16]	3.32[−16]	0.92
200	9.37[−17]	8.66[−17]	0.92
300	3.47[−17]	3.30[−17]	0.95
400	1.53[−17]	1.47[−17]	0.96
500	7.48[−18]	7.32[−18]	0.98
600	3.96[−18]	3.94[−18]	0.99
700	2.23[−18]	2.26[−18]	1.01
800	1.32[−18]	1.35[−18]	1.02
900	8.11[−19]	8.46[−19]	1.04
1000	5.16[−19]	5.46[−19]	1.06
1500	7.75[−20]	8.69[−20]	1.12
2000	1.75[−20]	2.04[−20]	1.16
3000	1.78[−21]	2.16[−21]	1.21
4000	3.12[−22]	3.88[−22]	1.24
5000	7.65[−23]	9.67[−23]	1.26
6000	2.35[−23]	3.00[−23]	1.28

TABLE III. Differential cross sections $dQ_{if}^{\mathrm{BDW}}/d\Omega \equiv (dQ_{if}^{\mathrm{BDW}\pm}/d\Omega)_{\mathrm{lab}}$ (cm^2/sr) as a function of the scattering angle $\theta \equiv \theta_{\mathrm{lab}}$ (mrad) at incident energy $E_{\mathrm{lab}} = 1.5$ MeV for double-charge exchange (3.1). The results are obtained by using the uncorrelated one-parameter Hylleraas [36] orbital $\varphi_{i,f}$ for helium and neglecting the correction (3.2).

θ_{lab}	$\left[\frac{dQ_{if}^{\mathrm{BDW}}}{d\Omega}\right]_{\mathrm{lab}}$	θ_{lab}	$\left[\frac{dQ_{if}^{\mathrm{BDW}}}{d\Omega}\right]_{\mathrm{lab}}$
0.0000	6.12[−13]	0.2250	7.67[−15]
0.0125	5.71[−13]	0.2300	7.62[−15]
0.0250	4.70[−13]	0.2400	7.45[−15]
0.0375	3.42[−13]	0.2500	7.20[−15]
0.0500	2.24[−13]	0.2750	6.37[−15]
0.0625	1.33[−13]	0.3000	5.44[−15]
0.0750	7.39[−14]	0.3250	4.57[−15]
0.0875	3.95[−14]	0.3500	3.82[−15]
0.1000	2.12[−14]	0.3750	3.18[−15]
0.1050	1.68[−14]	0.4000	2.65[−15]
0.1100	1.36[−14]	0.4250	2.21[−15]
0.1150	1.12[−14]	0.4500	1.84[−15]
0.1200	9.41[−15]	0.4750	1.55[−15]
0.1250	8.16[−15]	0.5000	1.30[−15]
0.1300	7.28[−15]	0.5250	1.10[−15]
0.1350	6.69[−15]	0.5500	9.32[−16]
0.1400	6.31[−15]	0.5750	7.94[−16]
0.1450	6.10[−15]	0.6000	6.80[−16]
0.1500	6.02[−15]	0.6250	5.85[−16]
0.1550	6.03[−15]	0.6500	5.05[−16]
0.1600	6.11[−15]	0.6750	4.39[−16]
0.1650	6.24[−15]	0.7000	3.82[−16]
0.1750	6.59[−15]	0.7250	3.34[−16]
0.1800	6.79[−15]	0.7500	2.94[−16]
0.1850	6.98[−15]	0.7750	2.59[−16]
0.1900	7.15[−15]	0.8000	2.29[−16]
0.1950	7.31[−15]	0.8250	2.03[−16]
0.2000	7.45[−15]	0.8500	1.81[−16]
0.2100	7.63[−15]	0.8750	1.62[−16]
0.2200	7.68[−15]	0.9000	1.45[−16]

considered in the present work, we shall neglect hereafter the correction φ_i'. In other words, our further reference to the BDW, BCIS, and CDW approximations will imply that the term $\zeta_i^+(H_T - E_i)\varphi_i$ is ignored from Eqs. (2.6), (2.8c), (2.9c), and (2.10). The results of such versions of the BDW, BCIS, and CDW approximations are shown in Tables III–V as well as in Figs. 1 and 2, together with the finding from the CB1 model. All four methods satisfy the correct boundary conditions in the entrance and exit channels of the general reaction (2.1). However, unlike the CB1 approach, the second-order BDW, BCIS, and CDW methods takes *full* account of the continuum intermediate states of both electrons in either the entrance and/or exit channels. Hence, by comparing the second-order theories with the CB1 approximation, we would learn about the relative importance of the intermediate electronic ionization continua. The outcome of such a comparison is evident and self-explanatory from Figs. 1 and 2. It is seen in Fig. 1 that the CB1 approximation exhibits an unphysical and experimentally unobserved dip at the scattering angle (called dark angle) $\theta_{\mathrm{lab}} \approx 0.1120$ mrad, which was already discussed. The same scalar perturbation potentials $Z_P(2/R - 1/s_1 - 1/s_2)$ is also present in the BCIS model (2.9c). However, here the contributions from the attractive and repulsive potentials do not cancel each other. In the dip region of the CB1 model, the angular distribution $dQ_{if}^{\mathrm{BCIS}}/d\Omega$ exhibits only a minimum at $\theta_{\mathrm{lab}} \approx 0.121$ mrad, followed by a neighboring broader maximum. The behavior of the angular distribution obtained in the BDW theory is altogether quite similar to that in the BCIS approximation [32]. For the reaction (3.1), the BDW and the BCIS model differ only in the perturbation potentials; the former contains the scalar product of the two *gradient* operators and the latter uses the *multiplicative* operators, as can be seen from Eqs. (2.6) and (2.9c). Both observables $dQ_{if}^{\mathrm{BDW}}/d\Omega$ and $dQ_{if}^{\mathrm{BCIS}}/d\Omega$, considered as a function of the scattering angle, are found to peak at the forward angle $\theta = 0.0$

TABLE IV. The total cross sections Q_{if} (cm^2) $\equiv Q_{if}^{\pm}$ (cm^2) as a function of the incident energy E_{lab} (keV) for the double-charge exchange (3.1). All the results refer to the four-body formalism of scattering theory, implemented through the use of the one-parameter Hylleraas [36] orbitals $\varphi_{i,f}$ for helium. The correction (3.2) is neglected. The present data: BDW (Born distorted-wave) and CDW (continuum distorted-wave) models. Also shown are the findings of the BCIS (boundary-corrected continuum intermediate state) [32] and CB1 (boundary-corrected first Born) [30] methods.

	Q_{if} (cm^2)			
E_{lab} (keV)	BDW	BCIS	CDW	CB1
900	1.54[−19]	1.89[−19]	3.21[−20]	8.11[−19]
1000	9.05[−20]	1.10[−19]	1.72[−20]	5.16[−19]
1250	2.70[−20]	3.19[−20]	4.34[−21]	1.87[−19]
1500	9.21[−21]	1.05[−20]	1.34[−21]	7.75[−20]
1750	3.51[−21]	3.89[−21]	4.81[−22]	3.54[−20]
2000	1.46[−21]	1.57[−21]	1.93[−22]	1.75[−20]
2500	3.14[−22]	3.17[−22]	4.00[−23]	5.10[−21]
3000	8.39[−23]	7.96[−23]	1.06[−23]	1.78[−21]
3500	2.64[−23]	2.37[−23]	3.37[−24]	7.07[−22]
4000	9.45[−24]	8.11[−24]	1.22[−24]	3.12[−22]
5000	1.61[−24]	1.31[−24]	2.17[−25]	7.65[−23]
6000	3.69[−25]	2.95[−25]	5.10[−26]	2.35[−23]
7000	1.03[−25]	8.69[−26]	1.46[−26]	8.55[−24]

mrad. The conventional Thomas double scattering for reaction (3.1) takes place at $\theta_{\rm lab}\approx 0.24$ mrad, but the impact energy of 1.5 MeV is too small to exhibit this effect clearly in the measurement, as well as in the BDW and BCIS methods. Despite the proper inclusion of the Rutherford scattering, the BDW and BCIS approximations predict the differential cross sections which are considerably lower than the corresponding experimental data of Schuch *et al.* [19] at larger scattering angles. More experimental and theoretical work is required to clarify this angular region of scattering. Nevertheless, differences observed between the measurement and the theory at these larger scattering angles θ will not be strongly apparent in the total cross sections, which are predominantly determined by collisions near the narrow forward direction. We did not presently attempt to perform any computations of the differential cross sections (2.11) by means of the four-body CDW model (CDW-4B). Instead we report the results obtained in the IPM version of the CDW approximation (CDW-IPM):

$$\frac{dQ_{if}^{\rm CDW\text{-}IPM}}{d\Omega}=\left|iv\mu_{PT}\int_0^\infty d\rho\,\rho^{1+2iv_{PT}}[\mathcal{A}_{if}^{\rm CDW\text{-}3B}(\rho)]^2\times J_{m_i-m_f}(\eta\rho)\right|^2\left[\frac{a_0^2}{sr}\right]. \quad (3.3)$$

Here, $\mathcal{A}_{if}^{\rm CDW\text{-}3B}(\rho)$ is the ρ-dependent transition ampli-

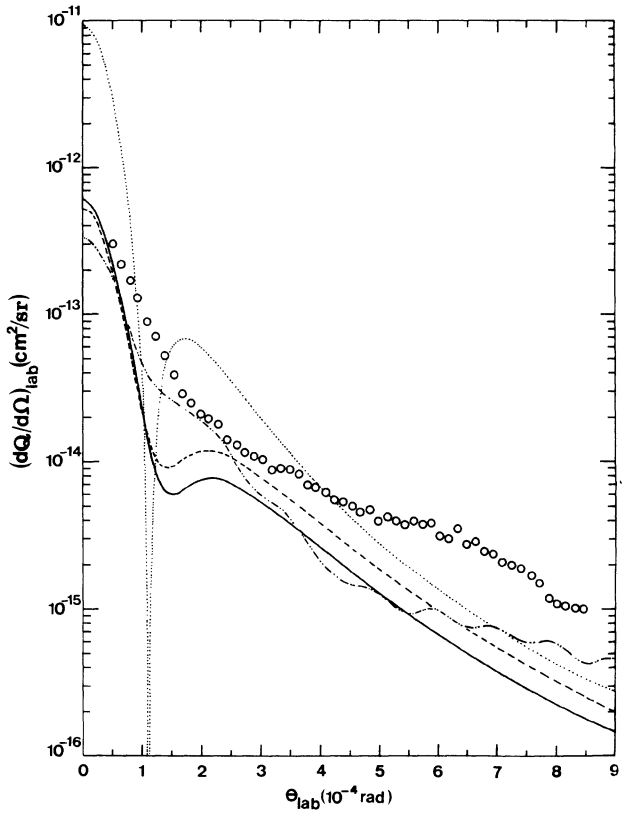

FIG. 1. Differential cross sections $(dQ/d\Omega)_{\rm lab}$ (cm^2/sr) as a function of scattering angle $\theta\equiv\theta_{\rm lab}$ (mrad) in the laboratory frame of reference at incident energy $E_{\rm lab}=1.5$ MeV for the double-charge exchange in α-He collision. The displayed theoretical curves relate only to the transition $1s^2\rightarrow 1s^2$, i.e., to process (3.1), for which there is no post-prior discrepancy. Theoretical results (all obtained using the one-parameter Hylleraas [36] orbitals of helium): (i) —— the Born distorted-wave approximation (present computation); (ii) — — —, the boundary-corrected continuum intermediate state method [32]; (iii) · · · ·, the boundary-corrected first Born model [30]; and (iv) –··–··–, the continuum distorted-wave independent-particle method (present computation). None of the quoted theoretical data are folded with the experimental resolution function. Experimental data (including double capture into all bound states of He): ○, Schuch *et al.* [19].

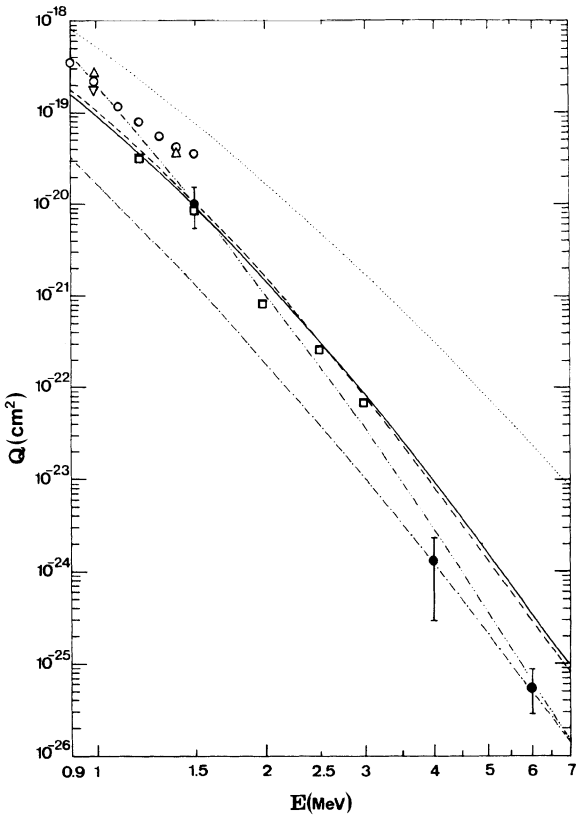

FIG. 2. Total cross sections, as a function of incident energy $E_{\rm lab}$ (MeV) for double-charge exchange reaction in α-He collision. The depicted theoretical curves relate only to the transition $1s^2\rightarrow 1s^2$, i.e., to reaction (3.1). Theoretical results (all obtained using the one-parameter Hylleraas orbitals [36] of helium): (i) ——, the Born distorted-wave approximation (present computation); (ii) — — —, the boundary-corrected continuum intermediate state method [32]; (iii) · · · ·, the boundary-corrected first Born model [30]; (iv) –··–··–, the continuum distorted-wave independent-particle method (present computation); and (v) —·—·—·, the four-body continuum distorted-wave approximation (present computation). Experimental data (including double capture into all bound states of He): ○, Pivovar, Novikov, and Tubaev [51]; △, McDaniel *et al.* [52]; ▽, DuBois [53]; □, de Castro Faria, Freire, and de Pinho [54]; and ●, Schuch *et al.* [19].

TABLE V. The present total cross sections $Q_{if}^{\text{CDW-4B}}$ (cm^2) as a function of the incident energy E_{lab} (keV) for the double-charge exchange (3.1). Columns headed by labels "Hylleraas," "Silverman," "Green," and "Löwdin" denote the results obtained by, respectively, using the Hylleraas [36], Silverman, Platas, and Matsen [48], Green *et al.* [49], and Löwdin [50] wave functions for both initial and final ground states $\varphi_{i,f}$. The correction (3.2) is neglected.

	$Q_{if}^{\text{CDW-4B}}$ (cm^2)			
E_{lab} (keV)	Hylleraas	Silverman	Green	Löwdin
100	5.31[−16]	6.07[−16]	5.58[−16]	5.49[−16]
200	4.28[−17]	4.50[−17]	4.37[−17]	4.28[−17]
300	8.18[−18]	8.11[−18]	8.19[−18]	7.99[−18]
400	2.25[−18]	2.14[−18]	2.23[−18]	2.17[−18]
500	7.70[−19]	7.08[−19]	7.54[−19]	7.33[−19]
600	3.03[−19]	2.72[−19]	2.95[−19]	2.86[−19]
700	1.33[−19]	1.17[−19]	1.28[−19]	1.25[−19]
800	6.32[−20]	5.44[−20]	6.06[−20]	5.88[−20]
900	3.21[−20]	2.72[−20]	3.06[−20]	2.97[−20]
1000	1.72[−20]	1.44[−20]	1.63[−20]	1.58[−20]
1250	4.34[−21]	3.54[−21]	4.09[−21]	3.98[−21]
1500	1.34[−21]	1.07[−21]	1.26[−21]	1.23[−21]
1750	4.81[−22]	3.79[−22]	4.53[−22]	4.40[−22]
2000	1.93[−22]	1.50[−22]	1.83[−22]	1.78[−22]
2500	4.01[−23]	3.08[−23]	3.92[−23]	3.80[−23]
3000	1.06[−23]	8.11[−24]	1.09[−23]	1.05[−23]
3500	3.37[−24]	2.56[−24]	3.62[−24]	3.74[−24]
4000	1.22[−24]	9.29[−25]	1.39[−24]	1.32[−24]
5000	2.17[−25]	1.65[−25]	2.72[−25]	2.55[−25]
6000	5.10[−26]	3.89[−26]	7.06[−26]	6.51[−26]
7000	1.46[−26]	1.12[−26]	2.21[−26]	2.01[−26]

tude in the original three-body CDW approximation of Cheshire [16] (for an explicit expression, see Belkić and Salin [35]). These results are seen from Fig. 1 to be in good agreement with the experimental data at small and intermediate scattering angles. At larger values of θ, this model also underestimates the measurement. There are some very pronounced undulations in $dQ^{\text{CDW-IPM}}/d\Omega$ at larger scattering angles. None of the theoretical data displayed in Fig. 1 are folded with the experimental resolution function. The folding procedure accounts for the geometrical properties of the detector mask, the rectangular beam dimensions, and the broadening of the incident beam profile, due to multiple elastic projectile scattering in the target gas. When this folding correction is introduced within, e.g., the CDW-IPM, it follows that the most important alterations occur in the forward direction, where folding reduces the cross section (3.3) by a factor ranging from ~ 3.1 at $\theta_{\text{lab}}=0.01$ mrad to ~ 1.2 at $\theta_{\text{lab}}=0.1$ mrad. At larger scattering angles the undulations are smoothed out by the folding procedure. The CDW-IPM was extended in Refs. [17,19] to include the configuration interaction (CI) model, which yields results quite similar to those originating from the uncorrelated Hylleraas [36] orbitals. Our folded angular distribution is in complete agreement with the previous computations of Deco and Grün reported in Refs. [17,19].

At sufficiently high impact energies, it should be possible to experimentally observe some intriguing higher-order effects in the prototype double-charge exchange (3.1). Applying the purely classical arguments [41], one expects to find a customary Thomas double scattering peak at the angle $\theta_{\text{lab}}^{(1)}=(1/m_P)\sin 60^\circ=(1/m_P)\sqrt{3}/2 \approx 0.118$ mrad $=0.0068^\circ$. This peak corresponds to two consecutive events: (i) one electron is captured through the direct first-order mechanism and (ii) the other electron is captured through the Thomas double scattering. The next analogous structure should occur at the angle $\theta_{\text{lab}}^{(2)}=2\theta_{\text{lab}}^{(1)}=(2/m_P)\sin 60^\circ=(1/m_P)\sqrt{3}\approx 0.236$ mrad $=0.0136^\circ$. Here, the two electrons treated classically are supposed to be "at the same time in the same place" to exhibit the cumulative Thomas double scattering. Each electron first scatters elastically on the projectile through 60° towards its parent nucleus. The subsequent scattering of each of the electrons on the target nucleus is also elastic through the next 60°. The two electrons are then ejected from the target with a velocity of the projectile in the incident beam direction. Hence the attractive force between Z_P and $2e$ suffices to bind these three particles together. Finally, yet another peak in $dQ/d\Omega$ is expected at the angle $\theta_{\text{lab}}^{(3)}=(1/m_P)\sqrt{2}\sin 45^\circ=(1/m_P)\approx 0.136$ mrad $=0.0078^\circ$, which is situated *between* $\theta_{\text{lab}}^{(1)}$ and $\theta_{\text{lab}}^{(2)}$. This time one electron (say e_1) is first scattered on the projectile through 45° towards the other electron (e_2) acquiring the velocity $v_1=\sqrt{v^2+v^2}=v\sqrt{2}$. Next, e_1 collides with e_2 elastically and finds itself deflected through another 45° in the incident beam direction with the velocity $v_1'=v$. The consequence of such an event on e_2 is manifested in the recoil of this second electron with the speed $v_2=v$ through 90° perpendicular to the incident

direction. In the final step, e_2 scatters elastically on the target nucleus through another 90° with $v_2'=v$ in the projectile direction. Then both electrons travel in the incident beam direction and are, therefore, captured by the projectile. This event producing the peak at $\theta_{\rm lab}^{(3)}$ represents a genuine *third-order* effect, which is hereafter termed as the Thomas *triple* scattering. Hence one should be able to record *three distinct structures* in the angular distribution $dQ/d\Omega$ for double-charge exchange. This is to be contrasted with the appearance of only one Thomas double scattering in single-electron capture from helium by fast projectiles, recently reported by Horsdal-Pedersen, Cocke, and Stockli [42]. This would provide a stringent test of the theory, particularly in view of the fact that the IPM versions of the peaking second Born and standard CDW-EIS approximations yield only two peaks [43]. The Thomas triple scattering at $\theta_{\rm lab}^{(3)}$ is a pure four-body effect due to *dynamic* interelectron correlations. In order to describe adequately these higher-order phenomena, it would probably be the most appropriate to use the full second- and third-order boundary-corrected Born (CB2,CB3) approximations in the four-body formalism. At sufficiently high energies (e.g., 5–10 MeV for $^4He^{2+}$-^4He double-charge exchange), it would be difficult to achieve the angular resolution required to experimentally observe the peak at $\theta_{\rm lab}^{(3)}$, which is superimposed onto the structure occurring at the angle $\theta_{\rm lab}^{(1)}$. However, the coincidence measurements of the scattered projectiles and the recoil He^+ ions [44] could be a powerful tool in providing valuable information about the Thomas scatterings in double-charge exchange and transfer ionization. Here, instead of the parameters of the projectile, one concentrates on the cross sections which are multiply differential in the momenta of the recoil ion. An unprecedented accuracy of the recoil spectroscopy technique in fully controlling the four-body kinematics should be more prominent when combined with the storage ring facilities. These latter measuring devices offer distinct advantages over any of the conventional single-pass experiments in regard to a high quality of beams, a substantially increased luminosity, and a tremendously reduced data taking time.

The total cross sections are presented in Fig. 2, from which we can see that the BDW and BCIS results are in overall good mutual agreement. At the same time, these two methods provide total cross sections which are much smaller than the corresponding results of the CB1 approximation throughout the energy range under consideration. The difference between the findings of the BDW and CB1 methods increases as the impact energy is augmented, reaching even *two orders* of magnitude at 6 MeV. Such a pattern is explained by the following argument. The two electrons are *intermediately* found in the on-shell continuum states of the projectile nucleus before the actual double capture takes place. Since the electrons are *not* staying in these continuum states in the *final* stage of the collision, the probability for double-electron transfer to a discrete state in the projectile Coulomb field is *reduced*. The obtained reduction seen in Fig. 2 is so significant that the mechanism of having the two electrons in the continuum intermediate states, as in the BDW method, becomes dominant over the simple picture of the CB1 model, according to which the electrons are *free* in the intermediate stage of collision involving double-charge exchange. If we account for the intermediate ionization continua symmetrically in both asymptotic channels, as done in (2.10) within the four-body CDW approximation [23,27], then the total cross section $Q_{if}^{\rm CDW}$ should be further reduced in relation to the BDW method. This is precisely what is observed in Fig. 2, with an explanation analogous to that put forward in the above discussion concerning the relation between the CB1 and BDW models. In Fig. 2, we also compare the theoretical and experimental results. It is seen from this comparison that the second-order BDW and BCIS methods yield an adequate description of the measurement. At the two largest energies (5 and 6 MeV), however, the BDW and BCIS models significantly overestimate the experimental data. This is partially due to the fact that these approximations allow for the full electronic continuum intermediate states only in *one* channel (entrance or exit). The other reason for a possible explanation of the discrepancy between the displayed second-order theories and the measurement at 5 and 6 MeV is an experimental underestimation of the true cross sections. Namely, the results reported in Ref. [19] at these two energies relate to the "partial" cross sections Q_p defined by $Q_p \equiv 2\pi \int_0^{\theta_m} d\theta (dQ/d\theta)$, where θ_m is a certain maximal value of the acceptance angle. Schuch *et al.* [19] have determined θ_m at 1.5 MeV, since they measured the differential cross sections at this energy. That same value of θ_m was also used at 5 and 6 MeV at which, however, no data on $dQ/d\theta$ were recorded by Schuch *et al.* [19]. A correction due to the proper determination of θ_m at 5 and 6 MeV could enlarge the error bar seen in Fig. 2 by another estimated amount of roughly 30%.

As to the four-body CDW model, we see in Fig. 2 that it completely fails to reproduce most of the experimental data, with the only exception for the two largest energies (4 and 6 MeV). The difference between the results of the BDW and CDW approximations is enormous throughout the energy range under investigation. This is at variance with a similar analysis made within these two methods for single-charge exchange at energies 1–10 MeV, which are comparable to those displayed in Fig. 2. We saw in Eqs. (2.6) and (2.10) that the prior variants of the BDW and CDW approximations coincide with each other only in the entrance channel. In the exit channel, the CDW approximation takes full account of the continuum intermediate states of the two electrons. In that channel, however, the BDW method completely ignores these *purely* electronic intermediate ionization continua and accounts only for the Coulombic distortion phase $\mathcal{F}_f = \exp[-(i/v)Z_T(Z_P-2)\ln(vR+\mathbf{v}\cdot\mathbf{R})]$ due to *elastic* scattering of the two scattering aggregates Z_T and $(Z_P,2e)_f$. We know that both initial and final total scattering wave functions of the CDW method are unnormalized at finite values of $r_{i,f}$. This introduces an *a priori* uncertainty in each of the scattering states. Such an error might be further augmented in the computation of the transition amplitude, since the initial and final

scattering states are projected onto each other. This type of "normalization error" is also present in the CDW method for single-charge exchange [45], but without a significant consequence at sufficiently high energies ($E \geq 80 \sup\{|E_i|, |E_f|\}$). This circumstance only indicates that the same type of errors invoked in theories of rearrangement collisions could be much more serious for double- than for single-charge exchange. The total cross sections at 1 and 6 MeV for two-electron transfer in α-He collision are, respectively, by two and six orders of magnitude smaller than the corresponding data for one-electron capture for the same scattering particles [46]. Therefore it is not surprising that double-charge exchange, as a much weaker effect, in comparison to the one-electron transfer, appears to be very sensitive to any, even apparently small, inadequacies of the theory. Concerning this "normalization problem," the situation is more favorable in the BDW model, since one of its total scattering states is properly normalized. This could be either the initial Φ_i^+ or final Φ_f^- configuration for the post or prior form of the transition amplitude, respectively. In Fig. 2 we also display the cross sections $Q_{if}^{\text{CDW-IPM}}$ presently obtained from (3.3) by the standard integration over ρ from zero to infinity (see also Refs. [17,19]). These results are in satisfactory agreement with measurement throughout the energy range 0.9–7 MeV, in contrast to the CDW-4B method. We have further performed additional computations within the CDW-IPM and obtained the cross sections $Q_{if}^{\text{CDW-IPM(ii)}}$ using the Hylleraas [36] wave function for φ_f and Roothaan-Hartree-Fock (RHF) orbital for φ_i, which is expressed in the analytical form of Clementi and Roetti [47]. These results are shown in Table VI, together with the cross sections $Q_{if}^{\text{CDW-IPM(i)}}$ computed with the help of the Hylleraas [36] orbital for *both* φ_i and φ_f. It is seen from this comparison that at lower-intermediate energies (1000–100 keV) the results for $Q_{if}^{\text{CDW-IPM(ii)}}$ are smaller than those for $Q_{if}^{\text{CDW-IPM(i)}}$ by a factor $\gamma' = Q_{if}^{\text{CDW-IPM(ii)}}/Q_{if}^{\text{CDW-IPM(i)}}$ ranging from 0.90 to 0.52 [see the column labeled by "Ratio" in Table VI]. Such a pattern is precisely reversed at higher energies from 1 to 7 MeV, at which $\gamma' = 0.90-1.65$. This trend is similar to the behavior of the corresponding ratio γ from Table II, but the variation of γ' is considerably more pronounced. The difference between columns (i) and (ii) from Table VI is a well-known consequence of the electronic correlations, whose radial effect is built to a quite large extent into the RHF orbital [47] and completely ignored in the Hylleraas [36] wave function.

In order to see how the total cross sections of the four-body theories are sensitive to the choice of the bound-state wave functions $\varphi_{i,f}$, we have selected the CDW-4B approximation to perform a detailed computation. Some of the high-energy results obtained using the simplest one-parameter orbitals of Hylleraas [36] are already displayed in Table IV. In Table V, these data are further compared with the findings obtained with the help of the two-, three-, and four-parameter orbitals $\varphi_{i,f}$, which are, respectively, due to Silverman, Platas, and Matsen [48], Green *et al.* [49], and Löwdin [50]. Despite their simplicity, these three latter configurations of the type $(1s1s')$ account for a large portion ($\sim 90\%$) of the radial correlation effects, in contrast to the $(1s)^2$ wave function of Hylleraas [36]. It is observed from Table V that the discrepancy between these four sets of results does not exceed 40%, at impact energies above 100 keV. A similar conclusion has previously been reached by Belkić and Mančev [27] in the case of H^+-He double-charge exchange studied within the CDW-4B.

TABLE VI. The present total cross sections $Q_{if}^{\text{CDW-IPM}}$ (cm^2) as a function of the incident energy E_{lab} (keV) for the double-charge exchange (3.1). Column (i): the Hylleraas [36] orbitals for $\varphi_{i,f}$. Column (ii): the Hartree-Fock [47] orbital for φ_i and the Hylleraas [36] orbital for φ_f. The third column is the ratio of the number in column (ii) to the one in (i).

E_{lab} (keV)	$Q_{if}^{\text{CDW-IPM}}$ (cm^2) (i)	(ii)	Ratio
100	4.75[−14]	2.48[−14]	0.52
200	2.00[−15]	1.36[−15]	0.68
300	2.67[−16]	1.98[−16]	0.74
400	5.78[−17]	4.49[−17]	0.78
500	1.64[−17]	1.32[−17]	0.80
600	5.58[−18]	4.61[−18]	0.83
700	2.15[−18]	1.82[−18]	0.85
800	9.15[−19]	7.91[−19]	0.86
900	4.19[−19]	3.70[−19]	0.88
1000	2.05[−19]	1.84[−19]	0.90
1500	1.08[−20]	1.07[−20]	0.99
2000	1.12[−21]	1.20[−21]	1.07
3000	3.68[−23]	4.50[−23]	1.22
4000	2.81[−24]	3.81[−24]	1.36
5000	3.55[−25]	5.21[−25]	1.47
6000	6.29[−26]	9.84[−26]	1.56
7000	1.42[−26]	2.34[−26]	1.65

IV. CONCLUSION

The problem of two-electron capture from helium by α particles is investigated at high energies by using the second-order four-body Born distorted-wave (BDW) and continuum distorted-wave (CDW) methods. The present computation of $dQ^{\text{BDW}}/d\Omega$ at 1.5 MeV reveals that these differential cross sections of the BDW approxima good agreement with the available experimental data in the vicinity of the forward direction. This method, however, considerably underestimates the measured findings for $dQ/d\Omega$ at larger scattering angles, despite the proper inclusion of the Rutherford scattering effects through the Coulomb phase factor of the internuclear repulsion. Further measurements on the angular distributions are necessary for a more thorough testing of various second-order theories. Comparison between the CB1 model and the BDW approximation revealed two important facts. The angular distribution obtained in the BDW theory does not exhibit the unphysical and experimentally unobserved extremely sharp dip, which is always present in the data of the CB1 model. The dip occurring at a so-called dark angle is due to a strong cancellation of the terms of opposite signs (attractive and repulsive interactions) in the perturbation potentials of the CB1 approach. However, the two terms of the above-mentioned gradient

operator form of the perturbation interaction in the BDW method provide the same contribution (in magnitude *and* sign) to the cross section. The energy of 1.5 MeV is too low to exhibit Thomas *multiple* scattering effects, which should manifest themselves in the appearance of *three* well-separated peaks.

As to the total cross sections, the CB1 approximation overestimates the experimental data by two orders of magnitude at the highest energies, but still below the region where Thomas scatterings become important. At the same time, the second-order BDW method is in overall satisfactory agreement with the measured total cross sections. This convincingly demonstrates that electronic intermediate ionization continua, which are included in the BDW and neglected in the CB1 model, play a crucial role in high-energy double-charge exchange.

However, the CDW approximation is found to underestimate most of the experimentally determined total cross sections by an order of magnitude. The reason for such an occurrence could stem from an eventual overaccount of the double electronic ionization continua and the possibly related augmentation of the "normalization error" of the distorted waves χ_i^+ and χ_f^+. However, if this turns out to be of unnoticeable numerical significance, the four-body CDW model for double-charge exchange could perhaps be improved by including the next term in the Dodd-Greider perturbation series expansion. Here, the real difficulty and challenge is to remove the hidden faults of the CDW method for double-charge exchange, without destroying the very comforting success of this model for single-electron capture. This fault, while perhaps always lying dormant in Chesire's original CDW theory, is brought to its full prominence only now, through a more stringent testing via a *higher-order* and *weaker* process, such as double-charge exchange. Hence much effort is required before a firm status of the theory for two-electron capture is settled in a satisfactory manner. More experiments are urgently needed to supply an extended data base for critical testing of various second-order theories.

ACKNOWLEDGMENTS

This work is carried out within a two-year research project of Dževad Belkić, supported by The Royal Swedish Academy of Sciences. He also wishes to thank Professor Anders Bárány and Professor Reinhold Schuch for several fruitful discussions.

[1] J. M. Hansteen and O. P. Mosebekk, Phys. Rev. Lett. **29**, 1361 (1972).
[2] J. H. McGuire and O. L. Weaver, Phys. Rev. A **16**, 41 (1977).
[3] S. C. Mukherjee, K. Roy, and N. C. Sil, J. Phys. B **6**, 467 (1973).
[4] S. Biswas, K. Bhadra, and D. Basu, Phys. Rev. A **15**, 1900 (1977).
[5] C. D. Lin, Phys. Rev. A **19**, 1510 (1979).
[6] T. C. Theisen and J. H. McGuire, Phys. Rev. A **20**, 1406 (1979).
[7] R. E. Olson, J. Phys. B **15**, L163 (1982).
[8] R. E. Olson, A. E. Wetmore, and M. L. McKenzie, J. Phys. B **19**, L629 (1986).
[9] R. Shingal and C. D. Lin, J. Phys. B **24**, 251 (1991).
[10] V. A. Sidorovich, V. S. Nikolaev, and J. H. McGuire, Phys. Rev. A **31**, 2193 (1985).
[11] D. S. F. Crothers and R. McCarroll, J. Phys. B **20**, 2835 (1987).
[12] K. M. Dunseath and D. S. F. Crothers, J. Phys. B **24**, 5003 (1991).
[13] N. C. Deb and D. S. F. Crothers, J. Phys. B **23**, L799 (1990).
[14] N. C. Deb and D. S. F. Crothers, J. Phys. B **24**, 2359 (1991).
[15] R. Gayet, R. D. Rivarola, and A. Salin, J. Phys. B **14**, 2421 (1981).
[16] I. M. Cheshire, Proc. Phys. Soc. London **84**, 89 (1964).
[17] G. Deco and N. Grün, Z. Phys. D **18**, 339 (1991).
[18] R. Gayet, J. Hanssen, A. Martinez, and R. Rivarola, Z. Phys. D **18**, 345 (1991).
[19] R. Schuch, E. Justiniano, H. Vogt, G. Deco, and N. Grün, J. Phys. B **24**, L133 (1991).
[20] M. Ghosh, C. R. Mandal, and S. C. Mukharjee, J. Phys. B **18**, 3797 (1985).
[21] M. Ghosh, C. R. Mandal, and S. C. Mukharjee, Phys. Rev. A **35**, 5259 (1987).
[22] K. J. Schaudt, N. H. Kwong, and J. D. Garcia, Phys. Rev. A **43**, 2294 (1991).
[23] Dž. Belkić and I. Mančev, Phys. Scr. **45**, 35 (1992).
[24] M. S. Gravielle and J. E. Miraglia, Phys. Rev. A **45**, 2965 (1992).
[25] H. Bachau, R. Gayet, J. Hanssen, and A. Zerarka, J. Phys. B **25**, 839 (1992).
[26] Dž. Belkić, R. Gayet, and A. Salin, Phys. Rep. **56**, 279 (1979).
[27] Dž Belkić and I. Mančev, Phys. Scr. **46**, 18 (1993).
[28] J. D. Dollard, J. Math. Phys. **5**, 729 (1964).
[29] Dž. Belkić and R. Gayet, J. Phys. B **10**, 1023 (1977).
[30] Dž. Belkić, Phys. Rev. A **47**, 189 (1993).
[31] Dž. Belkić, J. Phys. B **26**, 497 (1993).
[32] Dž. Belkić, Phys. Rev. A **47**, 3824 (1993).
[33] Dž. Belkić, Nucl. Instrum. Methods Phys. Res. B (to be published).
[34] Dž. Belkić and A. Salin, J. Phys. B **9**, L517 (1976).
[35] Dž. Belkić and A. Salin, J. Phys. B **11**, 3905 (1978).
[36] E. Hylleraas, Z. Phys. **54**, 347 (1929).
[37] C. L. Pekeris, Phys. Rev. **112**, 1649 (1958).
[38] Dž. Belkić, S. Saini, and H. S. Taylor, Z. Phys. D **3**, 59 (1986).
[39] K. E. Banyard and G. W. Shirtcliffe, J. Phys. B **12**, 3247 (1977).
[40] G. W. Shirtcliffe and K. E. Banyard, Phys. Rev. B **21**, 1197 (1980).
[41] R. Schuch, in *High-Energy Ion-Atom Collisions. Proceedings of the Third Workshop on High-Energy Ion-Atom Collisions, held in Debrecen, Hungary, August 3–5, 1987,* edited by D. Berényi and G. Hock, Lecture Notes in Physics

Vol. 294 (Springer-Verlag, Berlin, 1990), p. 297.
[42] E. Horsdal-Pedersen, C. L. Cocke, and M. Stockli, Phys. Rev. Lett. **50**, 1910 (1983).
[43] A. E. Martinez, R. Gayet, J. Hanssen, and R. D. Rivarola, in *18th International Conference on the Physics of Electronic and Atomic Collisions, Aarhus, Denmark, 1993, Abstracts of Contributed Papers,* edited by T. Andersen, B. Fastrup, F. Folkmann, and H. Knudsen (Aarhus University, Aarhus, 1993), Vol. 2, p. 602.
[44] R. Dörner, J. Ullrich, H. Schmidt-Böcking, and R. E. Olson, Phys. Rev. Lett. **63**, 147 (1989).
[45] D. S. F. Crothers, J. Phys. B **15**, 2061 (1982).
[46] Dž. Belkić, Phys. Scr. **40**, 610 (1989).
[47] E. Clementi and C. Roetti, At. Data Nucl. Data Tables **14**, 177 (1974).
[48] J. N. Silverman, O. Platas, and F. A. Matsen, J. Chem. Phys. **32**, 1402 (1960).
[49] L. C. Green, M. M. Mulder, M. N. Lewis, and J. Woll, Phys. Rev. **93**, 757 (1954).
[50] P. Löwdin, Phys. Rev. **90**, 120 (1953).
[51] L. I. Pivovar, M. T. Novikov, and V. M. Tubaev, Zh. Eksp. Teor. Fiz. **42**, 1490 (1962) [Sov. Phys. JETP **15**, 1035 (1962)].
[52] E. W. McDaniel, M. R. Flannery, H. W. Ellis, F. L. Eisele, and W. Pope, US Army Missile Research and Development Command Technical Report H, 1977 (unpublished).
[53] R. D. DuBois, Phys. Rev. A **36**, 2585 (1987).
[54] N. V. de Castro Faria, F. L. Freire, Jr., and A. G. de Pinho, Phys. Rev. A **37**, 280 (1988).